

Wavelength-tunable and high-temperature lasing in ZnMgO nanoneedles

H. Y. Yang, S. P. Lau,^{a)} and S. F. Yu

School of Electrical and Electronic Engineering, Nanyang Technological University, Nanyang Avenue, Singapore 639798, Singapore

M. Tanemura, T. Okita, and H. Hatano

Department of Environmental Technology, Graduate School of Engineering, Nagoya Institute of Technology, Gokiso-cho, Showa-ku, Nagoya 466-8555, Japan

K. S. Teng and S. P. Wilks

Multidisciplinary Nanotechnology Centre, School of Engineering, University of Wales Swansea, Singleton Park, Swansea SA2 8PP, United Kingdom

(Received 22 March 2006; accepted 2 July 2006; published online 22 August 2006)

Zn_{1-x}Mg_xO nanoneedles were prepared by an ion-beam technique on Zn_{1-x}Mg_xO thin films with Mg contents of up to 21 at.%. The photoluminescence emission energies of the Zn_{1-x}Mg_xO nanoneedles measured at room temperature increased monotonically with Mg contents and it reached 3.6 eV when $x=0.21$. Random laser action was observed in the Zn_{1-x}Mg_xO nanoneedles with $x \leq 0.1$ at temperature ranging from 300 to 470 K under 355 nm optical excitation. The characteristic temperature of the Zn_{1-x}Mg_xO nanoneedles was determined to be 84 K. The high-temperature lasing of the Zn_{1-x}Mg_xO nanoneedles are attributed to the high crystal quality of the nanoneedles, enhancement of oscillator strength in nanostructures, and a self-compensation mechanism in random laser cavities. © 2006 American Institute of Physics.

[DOI: 10.1063/1.2338525]

One-dimensional (1D) ZnO nanostructures have motivated intense fundamental research and technological development of low-threshold ultraviolet (UV) semiconductor lasers.¹ Alloying ZnO with Mg permits the band gap to be increased from 3.3 to 4.0 eV.² Thus, shorter wavelength lasers based on Zn_{1-x}Mg_xO could be developed. Despite the significant progress in the investigations of 1D ZnO nanostructures, there are only a few reports on Zn_{1-x}Mg_xO nanostructures but stimulated emission or lasing from these materials have not been reported.^{3,4} In this letter, we report the random laser action in Zn_{1-x}Mg_xO nanoneedles and demonstrate the wavelength-tunable lasers through controlling the Mg concentration. In addition, the high-temperature dependence of emission characteristics of Zn_{1-x}Mg_xO nanoneedles was also studied.

Zn_{1-x}Mg_xO thin films were grown by the filtered cathodic vacuum arc technique at 300 °C on Si substrates using various ZnMg alloy targets containing 15, 20, and 25 at. % of Mg. The typical arc current and deposition pressure were 60 A and 1.3×10^{-2} Pa, respectively. The corresponding Mg content in the Zn_{1-x}Mg_xO films was determined by x-ray photoelectron spectroscopy to be 7.8, 10, and 21 at. %, respectively. The Zn_{1-x}Mg_xO nanoneedles were fabricated by an ion-beam sputtering technique using a 3 keV Ar⁺ ion microbeam in an ultrahigh vacuum scanning electron microscope (SEM). Ion irradiation was carried out at room temperature for 30 min with mean ion-current densities of 220 $\mu\text{A}/\text{cm}^2$. The detailed fabrication procedures of nanoneedles have been described elsewhere.⁵

Figure 1(a) shows the cross-sectional transmission electron microscopy (TEM) image of Zn_{0.922}Mg_{0.078}O nanoneedle arrays. The nanoneedles were oriented in the ion-beam direction, which is 55° from the surface normal of a sample,

as labeled by the dashed arrows. As the Zn_{0.922}Mg_{0.078}O thin film was only 300 nm thick, the upper part of the cone was Zn_{0.922}Mg_{0.078}O (black contrast) and the lower part of the stem was SiO₂. Figure 1(b) shows the high-resolution TEM image at the interface of Zn_{0.922}Mg_{0.078}O and SiO₂. The corresponding selective area electron diffraction pattern illustrates the high crystal quality and wurtzite structure of the Zn_{0.922}Mg_{0.078}O sample. The lattice spacing in (002) direction of the Zn_{0.922}Mg_{0.078}O was found to be about 5.18 Å. Figure 1(c) shows the SEM image of the Zn_{0.922}Mg_{0.078}O nanoneedles sample. The lengths of the cone structure range from 200 to 400 nm. The diameter of the nanoneedles in the stem part was around 100 nm, where some of the nanoneedles

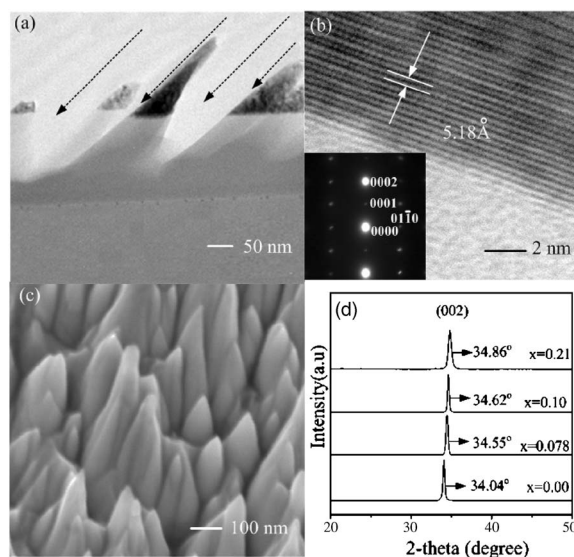


FIG. 1. (a) TEM image of the Zn_{0.922}Mg_{0.078}O nanoneedles. (b) High-resolution TEM image of the nanoneedle and the corresponding selected area electron diffraction pattern. (c) Typical SEM image of the Zn_{0.922}Mg_{0.078}O nanoneedles. (d) X-ray diffraction patterns of the ZnO and Zn_{1-x}Mg_xO nanoneedles.

^{a)} Author to whom correspondence should be addressed; electronic email: esplau@ntu.edu.sg

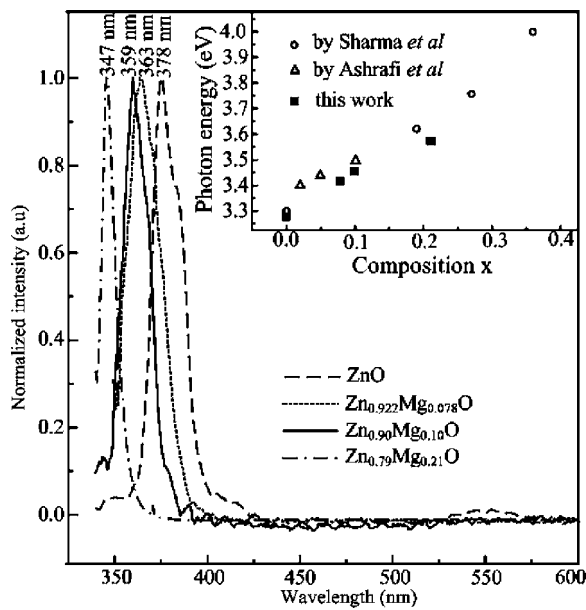


FIG. 2. Normalized PL spectra of the $Zn_{1-x}Mg_xO$ nanoneedles with various Mg contents. The inset shows the PL peak energy as a function of composition x of the $Zn_{1-x}Mg_xO$ nanoneedles. The PL data obtained from Refs. 6 and 7 are also included for comparison.

eedles tend to form in a cluster with similar sharpness at the tip. The crystal structure and orientation of the as-grown films were investigated by x-ray diffraction (XRD) measurement. Figure 1(d) shows the XRD spectra of $Zn_{1-x}Mg_xO$ films with various Mg contents. All the spectra exhibited only (002) peak, which revealed single phase, wurtzite structure and c -axis oriented $Zn_{1-x}Mg_xO$ films. The (002) peak position is shifted to higher angles as Mg content increases, which indicates that Mg ions are substituted into ZnO. Similar trend has also been observed by Ashrafi and Segawa,⁶ however, the angle shifted in our work is more than that of their work for the same Mg concentration. The discrepancies could be attributed to the different substrates used (Si versus SiC), stress, and crystal quality of the $Zn_{1-x}Mg_xO$ films.

Figure 2 shows the normalized room temperature photoluminescence (PL) spectra of the $Zn_{1-x}Mg_xO$ nanoneedles. The samples were excited by a 325 nm He-Cd laser at room temperature. The observed PL peak wavelengths of $Zn_{1-x}Mg_xO$ nanoneedles with 0, 7.8, 10, and 21 at. % of Mg

are 378, 363, 359, and 347 nm, respectively. The inset in Fig. 2 shows the variation of PL peak energies as a function of Mg composition. The PL data obtained from Refs. 6 and 7 were also included for comparison. Our results are in good agreement with their works. The PL peak energy of $Zn_{0.79}Mg_{0.21}O$ nanoneedles is blueshifted for 300 meV as compared to ZnO nanoneedles (PL peak energy = 3.28 eV).⁵ The full width at half maximum (FWHM) values of the samples are all less than 19 nm. It is also noted that no defect-related green emission can be observed from our $Zn_{1-x}Mg_xO$ nanoneedles although an extremely weak band at around 550 nm can be observed from the ZnO sample.

The optical characteristics of the $Zn_{1-x}Mg_xO$ samples were further carried out by a 355 nm frequency-tripled neodymium-doped yttrium aluminum garnet (10 Hz, 6 ns) pulse laser. A pumping stripe of length 8 mm and width 10 μ m was focused onto the surface of the sample by a cylindrical lens. Laser action in $Zn_{1-x}Mg_xO$ nanoneedles with Mg content of up to 10 at. % can be obtained. Due to the large band gap (3.58 eV) of the $Zn_{0.79}Mg_{0.21}O$ sample, our laser with energy of 3.5 eV is not sufficient to excite this sample. The typical lasing spectra of the $Zn_xMg_{1-x}O$ thin films at room temperature are exemplified in Fig. 3 for x value of ~ 0.10 , showing lasing modes centered at 378 nm. When the pump power reached a threshold value, a dramatic emission oscillation with coherent feedback emerged from the single broad emission spectra of all the samples at room temperature. The FWHM of the lasing peaks from all the samples remain less than 0.4 nm. The lasing emissions arise from the closed loop path of light formed by the $Zn_{1-x}Mg_xO$ nanoneedles. At higher excitation intensities above the threshold, more lasing modes are excited and these lasing actions can be detected in all directions. The lasing characteristics detected from the $Zn_{1-x}Mg_xO$ samples are similar to ZnO nanoneedles.⁵ Based on the structural properties of the $Zn_{1-x}Mg_xO$ nanoneedles and random laser theory, the observed lasing phenomena are attributed to random laser action.^{8,9} It should be noted that no lasing can be observed from the $Zn_{1-x}Mg_xO$ thin films without nanostructures. The insets in Fig. 3(a) show the plots of emission intensity versus pumping intensity (i.e., light-light curve), suggesting the clear onset of lasing emission. The lasing threshold of the $Zn_{0.922}Mg_{0.078}O$ ($Zn_{0.9}Mg_{0.1}O$) was ~ 0.30 MW/cm²

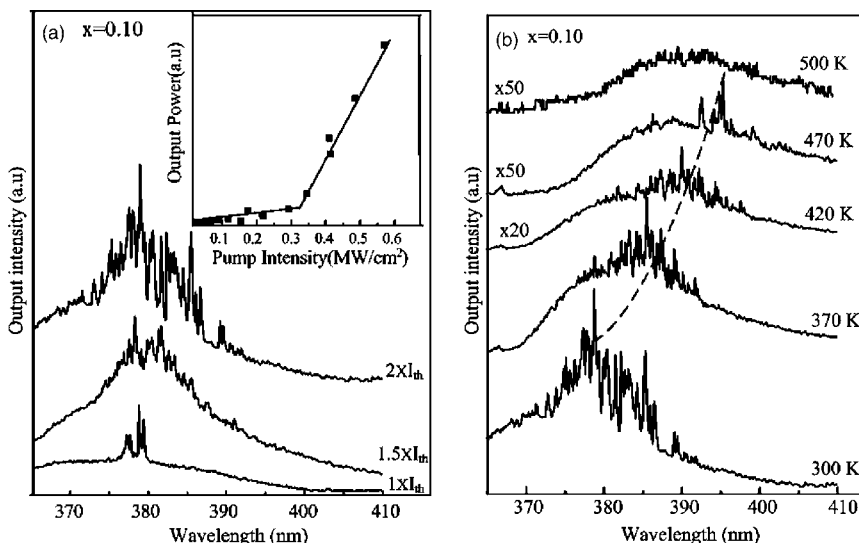


FIG. 3. (a) Room temperature lasing emission spectra at different excitation intensities from the $Zn_{0.90}Mg_{0.10}O$ nanoneedles. The inset shows the corresponding light-light curve of the sample. (b) Lasing emission spectra at different temperatures from the $Zn_{0.90}Mg_{0.10}O$ nanoneedles; the emission spectra were obtained under an excitation density of $2 \times I_{th}$.

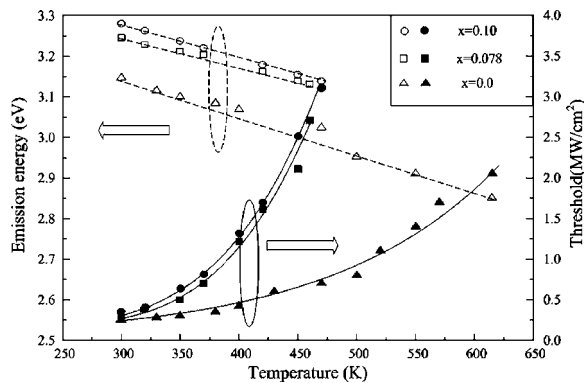


FIG. 4. Temperature dependence of lasing peak emission and lasing threshold of the $\text{Zn}_{1-x}\text{Mg}_x\text{O}$ nanoneedles, for $x=0$, 0.078, and 0.1. The solid line represents the best result of the least-squares fit to the experimental data.

($\sim 0.33 \text{ MW/cm}^2$) at room temperature which is comparable to ZnO nanoneedles.⁵

High-temperature lasing characteristics in ZnO based materials are scarce.^{10,11} Thus, the temperature dependence of lasing emission from the $\text{Zn}_{1-x}\text{Mg}_x\text{O}$ nanoneedles was investigated. Figure 3(b) shows the typical lasing spectra versus temperature T under optical excitation of $\sim 2 \times I_{\text{th}}$, where I_{th} represents the pump threshold at the corresponding T . With increasing temperature, the band gap of $\text{Zn}_{1-x}\text{Mg}_x\text{O}$ decreases which redshift the lasing peaks. The peak lasing wavelength of $\text{Zn}_{0.9}\text{Mg}_{0.1}\text{O}$ was redshifted from ~ 378 to $\sim 394 \text{ nm}$ as the temperature increased from 300 to 470 K. The lasing emission ceased when the temperature reached 470 K, however, a broad amplified spontaneous emission band remained. The FWHM of the lasing peaks for both samples remains less than 0.4 nm for temperature up to 470 K. Figure 4 plots the peak lasing emission of the $\text{Zn}_{1-x}\text{Mg}_x\text{O}$ nanoneedles as a function of temperature. The emission peak of the $\text{Zn}_{0.922}\text{Mg}_{0.078}\text{O}$ ($\text{Zn}_{0.9}\text{Mg}_{0.1}\text{O}$) nanoneedles were redshifted from $\sim 3.24 \text{ eV}$ ($\sim 3.28 \text{ eV}$) to 3.14 eV ($\sim 3.15 \text{ eV}$) at a rate of -0.67 meV/K (-0.82 meV/K) from room temperature to 470 K. The observed linear relationship between the emission peak energy and temperature of our $\text{Zn}_{1-x}\text{Mg}_x\text{O}$ nanoneedles is in good agreement with the electron-hole plasma stimulated emission observed from ZnO thin film on sapphire substrate.¹²

The lasing threshold of the $\text{Zn}_{1-x}\text{Mg}_x\text{O}$ nanoneedles was measured as a function of temperature and plotted in Fig. 4 for $x=0$, 0.078, and 0.1. It was found that the I_{th} of the $\text{Zn}_{1-x}\text{Mg}_x\text{O}$ nanoneedles increased exponentially with temperature. The solid line represents the best fit using least-squares fitting of the experimental data to the empirical formula: $I_{\text{th}}(T)=I_0 \exp(T/T_c)$ for the temperature dependence of the threshold, where I_0 is the threshold pump intensity at $T=0 \text{ K}$ and T_c is the characteristic temperature.¹³ The T_c of the ZnO, $\text{Zn}_{0.922}\text{Mg}_{0.078}\text{O}$, and $\text{Zn}_{0.9}\text{Mg}_{0.1}\text{O}$ samples was determined to be 138, 81, and 84 K, respectively. The T_c of the $\text{Zn}_{1-x}\text{Mg}_x\text{O}$ nanoneedles was significantly higher than that of ZnO/sapphire (67 K) and was comparable to ZnO/ $\text{Zn}_{0.74}\text{Mg}_{0.26}\text{O}$ superlattice on ScAlMgO_4 (87 K).¹⁰ However, the T_c of the ZnO nanoneedles is much higher than that of the $\text{Zn}_{1-x}\text{Mg}_x\text{O}$ nanoneedles, which could be attributed to the higher exciton binding energy of ZnO and higher optical gain in the ZnO nanoneedles as compared with $\text{Zn}_{1-x}\text{Mg}_x\text{O}$ nanoneedles. The relatively high values of lasing thresholds in the temperature range effectively eliminate

exciton-related effects from consideration of laser mechanisms. The free carrier recombination or electron-hole plasma is the dominant lasing mechanism in the $\text{Zn}_{1-x}\text{Mg}_x\text{O}$ for temperature above 300 K.

Several factors are believed to contribute to the high operating temperature of the $\text{Zn}_{1-x}\text{Mg}_x\text{O}$ lasers, including (1) the high optical quality of the structures, (2) the enhancement of oscillator strength in 1D nanostructure,¹⁴ and (3) the self-compensation ability of random laser cavities.¹¹ In our case, the nanoneedles are of high crystal quality and free of defect-related emission, which ensure a high optical gain in the structure. Furthermore, the optical gain can be increased because of the enhancement of oscillator strength in 1D nanostructure. This modified density of states should result in a narrower spread of carriers in energy, a high peak gain, and thus better temperature stability. As reported by Li *et al.*,¹¹ the average cavity length of a random laser will be reduced as an increase in temperature in order to sustain lasing at high temperature. Similarly the high-temperature random laser action in the $\text{Zn}_{1-x}\text{Mg}_x\text{O}$ nanoneedles should also be governed by the self-compensation mechanism in laser cavities.

In summary, we have demonstrated the wavelength-tunable PL and lasing emission from 1D $\text{Zn}_{1-x}\text{Mg}_x\text{O}$ nanoneedles. Changing temperature allows further “tuning” of the lasing peak energy. The T_c of the $\text{Zn}_{0.922}\text{Mg}_{0.078}\text{O}$ and $\text{Zn}_{0.9}\text{Mg}_{0.1}\text{O}$ samples were 81 and 84 K, respectively. The dominant lasing mechanism in $\text{Zn}_{1-x}\text{Mg}_x\text{O}$ for temperature above 300 K is believed to be electron-hole plasma.

This work was partly supported by the Agency for Science, Technology and Research of Singapore (ASTAR* Project No. 022-101-0033), the Japan Society for the Promotion of Science (JSPS; Grants-in-Aid for Scientific Research B, No. 15360007), and the NITECH 21st Century COE Program “World Ceramics Center for Environmental Harmony.”

¹M. H. Huang, S. Mao, H. Feich, H. Yan, Y. Wu, H. Kind, E. Weber, R. Russo, and P. Yang, *Science* **292**, 1897 (2001).

²A. Ohtomo, M. Kawasaki, T. Koida, K. Masubuchi, H. Koinuma, Y. Sakurai, Y. Yoshida, T. Yasuda, and Y. Segawa, *Appl. Phys. Lett.* **72**, 2466 (1998).

³M. Lorenz, E. M. Kaidashev, A. Rahm, Th. Nobis, J. Lenzner, G. Wagner, D. Spemann, H. Hochmuth, and M. Grundmann, *Appl. Phys. Lett.* **86**, 143113 (2005).

⁴R. Kling, C. Kirchner, T. Gruber, F. Reuss, and A. Waag, *Nanotechnology* **15**, 1043 (2004).

⁵S. P. Lau, H. Y. Yang, S. F. Yu, H. D. Li, M. Tanemura, T. Okita, H. Hatano, and H. H. Hng, *Appl. Phys. Lett.* **87**, 013104 (2005).

⁶A. B. M. A. Ashrafi and Y. Segawa, *J. Vac. Sci. Technol. B* **23**, 2030 (2005).

⁷A. K. Shama, J. Narayan, J. F. Muth, C. W. Teng, C. Jin, A. Kvit, R. M. Kolbas, and O. W. Holland, *Appl. Phys. Lett.* **75**, 3327 (2005).

⁸S. P. Lau, H. Y. Yang, S. F. Yu, C. Yuen, E. S. P. Leong, H. D. Li, and H. H. Hng, *Small* **1**, 956 (2005).

⁹H. Cao, *Waves Random Media* **12**, R1 (2003).

¹⁰A. Ohtomo, K. Tamura, M. Kawasaki, T. Makino, Y. Segawa, Z. K. Tang, G. K. L. Wong, Y. Matsumoto, and H. Koinuma, *Appl. Phys. Lett.* **77**, 2204 (2000).

¹¹H. D. Li, S. F. Yu, S. P. Lau, E. S. P. Leong, H. Y. Yang, T. Chen, A. P. Abiyasa, and C. Y. Ng, *Adv. Mater. (Weinheim, Ger.)* **18**, 771 (2006).

¹²D. M. Bagnall, Y. F. Chen, Z. Zhu, T. Yao, M. Y. Shen, and T. Goto, *Appl. Phys. Lett.* **73**, 1038 (1998).

¹³S. Bidnyk, T. J. Schmidt, Y. H. Gho, G. H. Gainer, J. J. Song, S. Keller, U. K. Mishra, and S. P. Denbaars, *Appl. Phys. Lett.* **72**, 1623 (1998).

¹⁴Y. Arakawa and H. Sakaki, *Appl. Phys. Lett.* **40**, 939 (1982).